Arbitrary-length XX spin chains boundary-driven by non-Markovian environments

G. Mouloudakis [1,2,*] T. Ilias [1,†] and P. Lambropoulos [1,2]

[1]*Department of Physics, University of Crete, P.O. Box 2208, GR-71003 Heraklion, Crete, Greece*

[2]*Institute of Electronic Structure and Laser, FORTH, P.O. Box 1527, GR-71110 Heraklion, Greece*

(Received 15 November 2021; accepted 14 January 2022; published 27 January 2022)

In this work we provide a recursive method of calculating the wave function of an XX spin chain coupled at both ends to non-Markovian reservoirs with arbitrary spectral density. The method is based on the appropriate handling of the time-dependent Schrödinger's equations of motion in Laplace space and leads to closed-form solutions of the transformed amplitudes for arbitrary chain lengths as well as arbitrary initial conditions within the single-excitation subspace. Results on the dynamical as well as state-transfer properties of the system for various combinations of parameters are also presented. In particular, detailed quantitative comparisons for Lorentzian and Ohmic reservoirs are illustrated.

DOI: 10.1103/PhysRevA.105.012429

I. INTRODUCTION

One-dimensional many-body systems such as quantum spin chains arise in many contexts throughout quantum information theory as well as condensed-matter physics due to their versatility as basic resources for the implementation of solid-state devices for quantum computing and quantum communication tasks [1]. Among these tasks, faithful quantum state transfer [2–9] and long-distance entanglement [10–15] have been investigated for various spin-chain configurations in great detail throughout the last 20 years or so, with the research in these fields being still active.

In recent years, much interest has arisen in the study of the properties of open quantum systems interacting with external environments, whose experimental realization inevitably involves decoherence and dissipation. Such systems may consist of just a pair of qubits, with a focus on the effects of the environmental dissipation on the generated bipartite entanglement [16–20], up to a whole quantum spin chain with focus on state transfer [21–24] or short- and long-distance correlations [25–28]. Extensions that account for the non-Markovian character of the surrounding environment have also been made [29–35], revealing interesting effects associated with the memory character of the reservoir, which enable the exchange of information between the system and the environment within finite times.

At the same time, attention has been drawn to a special class of open quantum systems, i.e., the so-called boundary-driven open quantum systems [36]. These are quantum systems coupled to external environments at their edges and are usually studied for their transport [37–40] and thermodynamic properties [41–43]. For one-dimensional boundary-driven open quantum systems, the different temperatures or chemical potentials between the two edge baths will cause a current flow from one bath to the other, mediated by the quantum system, which can reach a nonequilibrium steady state (NESS). The study of the transport properties of such systems, focusing on ways to control the associated current flows efficiently, therefore seems promising owing to the potential applications in solid-state devices such as diodes or transistors [44]. On the other hand, the dynamical and quantum state-transfer properties of such systems [45] are also essential from a practical perspective for the implementation of quantum information tasks.

Among the tools available for the study of open quantum systems, tensor network numerical methods based on matrix product states have proven quite efficient for the simulation of their dynamical behavior [46,47]. The method of matrix product states can, in many cases, yield analytical expressions for the expectation values of observables in the NESS of open quantum systems boundary-driven by Lindblad operators for Markovian reservoirs [48–51]. Perturbative approaches [52] as well as approaches based on quantum trajectories using numerical Monte Carlo techniques [53] have also been explored in great detail.

In this paper, we extend the study of the dynamics of an arbitrary-length XX chain boundary-driven by two non-Markovian reservoirs. Our theory is cast in terms of Schrödinger's equations of motion within the single-excitation subspace, which can be solved recursively in Laplace space, yielding closed-form solutions for the transformed amplitudes for a broad class of spectral densities of the boundary reservoirs, as well as arbitrary initial conditions. Results for the quantum state-transfer properties of the system for various parameters of the two reservoirs are also presented. Our work extends the analytical techniques used for dealing with boundary-driven open quantum systems by providing a systematic way of calculating the whole wave function of the spin chain and therefore enabling the study of numerous properties of the system at hand.

*gmouloudakis@physics.uoc.gr

†Present Address: Institut für Theoretische Physik, Albert-Einstein-Allee 11, Universität Ulm, D-89069 Ulm, Germany.

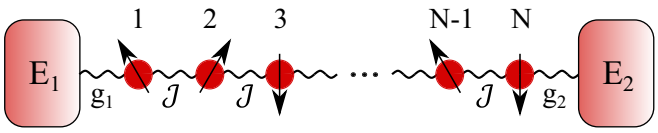

FIG. 1. Schematic presentation of the system under study. A Heisenberg XX spin chain of arbitrary length is coupled to non-Markovian reservoirs at its boundaries.

In much of the extensive literature on methods for the handling of non-Markovian reservoirs, the Lorentzian or Ohmic spectral densities are used for illustration. Yet the analytical forms of those spectral densities are fairly different. In order to explore the impact of those forms on the behavior of realistic physical systems, we have, in addition, performed comparative calculations for those two reservoirs. Our results, discussed in Sec. III, seem to reveal what one might call differences in the Markovianity of the two reservoirs.

This article is organized as follows: In Sec. II we provide the theoretical description of our problem in terms of the time-dependent Schrödinger equation (TDSE) and obtain closed-form solutions for the transformed amplitudes for an arbitrary number of sites, arbitrary spectral densities of the boundary reservoirs, and arbitrary initial conditions within the single-excitation subspace. In Sec. III we illustrate the potential of our approach through the application to two types of non-Markovian boundary reservoirs, namely, Lorentzian and Ohmic, by studying the dynamical or state-transfer properties of the system, and in Sec. IV we provide some concluding remarks as well as future directions related to our work.

II. THEORY

Our system consists of an N qubit (spin) chain interacting with two environments, E_1 and E_2, through its first and last qubits, with coupling strengths g_1 and g_2, respectively. The interaction between each pair of neighboring qubits in the chain is denoted by $\mathcal{J}$. A schematic presentation of our system is depicted in Fig. 1. The Hamiltonian of our system $\mathcal{H} = \mathcal{H}_S + \mathcal{H}_E + \mathcal{H}_I$ consists of three parts, namely, the Hamiltonian of the XX chain $\mathcal{H}_S$, the Hamiltonian of the two environments $\mathcal{H}_E$, and the chain-environment-interaction Hamiltonian $\mathcal{H}_I$, given by the relations ($\hbar = 1$)

$$\mathcal{H}_S = \omega_e \sum_{i=1}^{N} |e\rangle_{i\,i}\langle e| + \omega_g \sum_{i=1}^{N} |g\rangle_{i\,i}\langle g| + \sum_{i=1}^{N-1} \frac{\mathcal{J}}{2}(\sigma_i^+\sigma_{i+1}^- + \sigma_i^-\sigma_{i+1}^+), \tag{1a}$$

$$\mathcal{H}_E = \sum_{\lambda} \omega_\lambda^1 a_\lambda^{E_1\dagger} a_\lambda^{E_1} + \sum_{\lambda} \omega_\lambda^2 a_\lambda^{E_2\dagger} a_\lambda^{E_2}, \tag{1b}$$

$$\mathcal{H}_I = \sum_{\lambda} g_1(\omega_\lambda^1)\left(a_\lambda^{E_1}\sigma_1^+ + a_\lambda^{E_1\dagger}\sigma_1^-\right) + \sum_{\lambda} g_2(\omega_\lambda^2)\left(a_\lambda^{E_2}\sigma_N^+ + a_\lambda^{E_2\dagger}\sigma_N^-\right), \tag{1c}$$

where ω_g and ω_e are, respectively, the energies of the ground and excited states of each spin (all spins are assumed to be identical), ω_λ^i ($i = 1, 2$) is the energy of the λ-mode photon of each environment, $a_\lambda^{E_j}$ and $a_\lambda^{E_j\dagger}$ ($j = 1, 2$) are the annihilation and creation operators of each environment, respectively, and $\sigma_i^+ = |e\rangle_{i\,i}\langle g|$ and $\sigma_i^- = |g\rangle_{i\,i}\langle e|$ ($i = 1, \ldots, N$) are the qubit raising and lowering operators, respectively.

The wave function of the compound system (spin chain + environments) in the single-excitation space is expressed as

$$|\Psi(t)\rangle = \sum_{i=1}^{N} c_i(t)|\psi_i\rangle + \sum_{\lambda} c_\lambda^{E_1}(t)\left|\psi_\lambda^{E_1}\right\rangle + \sum_{\lambda} c_\lambda^{E_2}(t)\left|\psi_\lambda^{E_2}\right\rangle, \tag{2}$$

where

$$|\psi_i\rangle = |g\rangle_1|g\rangle_2\cdots|g\rangle_{i-1}|e\rangle_i|g\rangle_{i+1}\cdots|g\rangle_N|0\rangle_{E_1}|0\rangle_{E_2}, \tag{3a}$$

$$\left|\psi_\lambda^1\right\rangle = |g\rangle_1|g\rangle_2\cdots|g\rangle_N|00\cdots01_\lambda0\ldots00\rangle_{E_1}|0\rangle_{E_2}, \tag{3b}$$

$$\left|\psi_\lambda^2\right\rangle = |g\rangle_1|g\rangle_2\cdots|g\rangle_N|0\rangle_{E_1}|00\cdots01_\lambda0\cdots00\rangle_{E_2}. \tag{3c}$$

For our derivation, it is useful to adopt the transformations $c_i(t) = e^{-i[\omega_e+(N-1)\omega_g]t}\tilde{c}_i(t)$ ($i = 1, \ldots, N$) and $c_\lambda^{E_j}(t) = e^{-i(N\omega_g+\omega_\lambda^j)t}\tilde{c}_\lambda^{E_j}(t)$ ($j = 1, 2$) for the qubits' and environments' amplitudes. The equations of motion of the transformed amplitudes, resulting from the TDSE, are

$$i\frac{d\tilde{c}_1(t)}{dt} = \frac{\mathcal{J}}{2}\tilde{c}_2(t) + \sum_{\lambda} g_1(\omega_\lambda^1)e^{-i\Delta_\lambda^1 t}\tilde{c}_\lambda^{E_1}(t), \tag{4a}$$

$$i\frac{d\tilde{c}_i(t)}{dt} = \frac{\mathcal{J}}{2}[\tilde{c}_{i-1}(t) + \tilde{c}_{i+1}(t)], \quad i = 2, \ldots, N-1, \tag{4b}$$

$$i\frac{d\tilde{c}_N(t)}{dt} = \frac{\mathcal{J}}{2}\tilde{c}_{N-1}(t) + \sum_{\lambda} g_2(\omega_\lambda^2)e^{-i\Delta_\lambda^2 t}\tilde{c}_\lambda^{E_2}(t), \tag{4c}$$

$$i\frac{d\tilde{c}_\lambda^{E_1}(t)}{dt} = g_1(\omega_\lambda^1)e^{i\Delta_\lambda^1 t}\tilde{c}_1(t), \tag{4d}$$

$$i\frac{d\tilde{c}_\lambda^{E_2}(t)}{dt} = g_2(\omega_\lambda^2)e^{i\Delta_\lambda^2 t}\tilde{c}_2(t), \tag{4e}$$

where $\Delta_\lambda^j \equiv \omega_\lambda^j - (\omega_e - \omega_g) \equiv \omega_\lambda^j - \omega_{eg}$, $j = 1, 2$.

Formal integration of Eqs. (4d) and (4e), under the assumption that $\tilde{c}_\lambda^{E_1}(0) = \tilde{c}_\lambda^{E_2}(0) = 0$, and substitution back into Eqs. (4a) and (4c) yield

$$\frac{d\tilde{c}_1(t)}{dt} = -i\frac{\mathcal{J}}{2}\tilde{c}_2(t) - \int_0^t \sum_{\lambda} e^{-i\Delta_\lambda^1(t-t')}\left[g_1(\omega_\lambda^1)\right]^2\tilde{c}_1(t')dt', \tag{5a}$$

$$\frac{d\tilde{c}_N(t)}{dt} = -i\frac{\mathcal{J}}{2}\tilde{c}_{N-1}(t) - \int_0^t \sum_{\lambda} e^{-i\Delta_\lambda^2(t-t')}\left[g_2(\omega_\lambda^2)\right]^2\tilde{c}_N(t')dt'. \tag{5b}$$

The summation over all possible modes of each environment can be replaced by an integration that requires the specification of the environment's spectral density $J_j(\omega_\lambda^j)$, according to $\sum_\lambda [g_j(\omega_\lambda^j)]^2 \to \int d\omega_\lambda^j J_j(\omega_\lambda^j)$, $j = 1, 2$. In what follows, we keep the spectral density of both environments arbitrary. The resulting set of differential equations then is

$$\frac{d\tilde{c}_1(t)}{dt} = -i\frac{\mathcal{J}}{2}\tilde{c}_2(t) - \int_0^t R_1(t-t')\tilde{c}_1(t')dt', \tag{6a}$$

$$\frac{d\tilde{c}_i(t)}{dt} = -i\frac{\mathcal{J}}{2}[\tilde{c}_{i-1}(t) + \tilde{c}_{i+1}(t)], \quad i = 2, \ldots, N-1, \tag{6b}$$

$$\frac{d\tilde{c}_N(t)}{dt} = -i\frac{\mathcal{J}}{2}\tilde{c}_{N-1}(t) - \int_0^t R_2(t-t')\tilde{c}_N(t')dt', \tag{6c}$$

where we have introduced the definition

$$R_j(t) \equiv \int_0^\infty J_j(\omega_\lambda^j)e^{-i\Delta_\lambda^j t}d\omega_\lambda^j, \quad j = 1, 2. \tag{7}$$

Taking now the Laplace transform of the above set of differential equations and using the property of the convolution transform, $\mathcal{L}[\int_0^t f(t')g(t-t')dt'] = F(s)G(s)$, where $F(s)$ and $G(s)$ are the Laplace transforms of functions $f(t)$ and $g(t)$, respectively, we obtain

$$sF_1(s) = c_1(0) - i\frac{\mathcal{J}}{2}F_2(s) - B_1(s)F_1(s), \tag{8a}$$

$$sF_i(s) = c_i(0) - i\frac{\mathcal{J}}{2}[F_{i-1}(s)+F_{i+1}(s)], \quad i=2,\ldots,N-1, \tag{8b}$$

$$sF_N(s) = c_N(0) - i\frac{\mathcal{J}}{2}F_{N-1}(s) - B_2(s)F_N(s), \tag{8c}$$

where we have used the fact that $\tilde{c}_i(0) = c_i(0)$ since $c_i(t) = e^{-i[\omega_e+(N-1)\omega_g]t}\tilde{c}_i(t)$. In the above system of algebraic equations, $F_i(s)$ is the Laplace transform of $\tilde{c}_i(t)$, while $B_j(s)$ is the Laplace transform of the function $R_j(t)$, $j = 1, 2$.

As detailed in the Appendix, the set of equations (8) can be organized in such a way that each $F_i(s)$, $i = 2, \ldots, N$, is expressed in terms of $F_1(s)$ as

$$F_i(s) = A_i(s)F_1(s) + A_{i-1}(s)(ik)B_1(s)F_1(s) - (ik)\sum_{n=1}^{i-1}A_{i-n}(s)c_n(0), \quad i = 2, \ldots, N, \tag{9}$$

where $k \equiv \frac{2}{\mathcal{J}}$ and $A_i(s)$ obey the relation

$$A_{m+2}(s) = (iks)A_{m+1}(s) - A_m(s), \quad m = 1, \ldots, N, \tag{10}$$

with $A_1(s) = 1$ and $A_2(s) = iks$. Given these conditions, one can easily verify that the mth term of this sequence is given by

$$A_m(s) = \frac{[(iks) + i\sqrt{k^2s^2+4}]^m - [(iks) - i\sqrt{k^2s^2+4}]^m}{2^m i\sqrt{k^2s^2+4}}, \quad m = 1, \ldots, N. \tag{11}$$

Taking Eq. (9) for $i = N-1$ and $i = N$, we obtain

$$F_{N-1}(s) = A_{N-1}(s)F_1(s) + A_{N-2}(s)(ik)B_1(s)F_1(s) - (ik)\sum_{m=1}^{N-2}A_{N-1-m}(s)c_m(0), \tag{12}$$

$$F_N(s) = A_N(s)F_1(s) + A_{N-1}(s)(ik)B_1(s)F_1(s) - (ik)\sum_{m=1}^{N-1}A_{N-m}(s)c_m(0). \tag{13}$$

Substituting Eqs. (12) and (13) back into Eq. (8c) and using the relation $\sum_{m=1}^{N-1}A_{N-m}(s)c_m(0) = \sum_{m=1}^{N-2}A_{N-m}(s)c_m(0) + A_1(s)c_{N-1}(0)$, we can, after some straightforward algebraic manipulations, find that $F_1(s)$ is given by

$$F_1(s) = \frac{ikc_N(0) - k^2[s+B_2(s)]A_1(s)c_{N-1}(0) + (ik)\sum_{m=1}^{N-2}\{ik[s+B_2(s)]A_{N-m}(s) - A_{N-1-m}(s)\}c_m(0)}{ik[s+B_2(s)]A_N(s) - \{1+k^2B_1(s)[s+B_2(s)]\}A_{N-1}(s) - ikB_1(s)A_{N-2}(s)}. \tag{14}$$

The inverse Laplace transform of Eq. (14) provides the time evolution of the amplitude $\tilde{c}_1(t)$. The rest of the amplitudes are given by the inverse Laplace transforms of $F_i(s)$, $i = 2, \ldots, N$ which are recursively related to $F_1(s)$ through Eq. (9).

The analytical method we developed above allows us to obtain the time evolution of the amplitude of any spin for an arbitrary number of sites as well as for arbitrary initial conditions within the single-excitation subspace by simply calculating the inversion integral of the corresponding Laplace transform. With our method, the number of sites N becomes an arbitrary and easily modifiable parameter entering expression (14). The inversion integral can be readily calculated numerically (or even analytically in some cases) after specification of the spectral density of each environment, which is necessary for the calculation of the Laplace transforms $B_j(s)$ of the functions $R_j(t)$.

III. RESULTS AND DISCUSSION

A. Lorentzian spectral density

As a first example, we consider the case of an XX chain boundary-driven by two non-Markovian reservoirs with Lorentzian spectral densities, given by

$$J_j(\omega_\lambda^j) = \frac{g_j^2}{\pi} \frac{\frac{\gamma_j}{2}}{\left(\omega_\lambda^j - \omega_c^j\right)^2 + \left(\frac{\gamma_j}{2}\right)^2}, \quad j = 1, 2, \tag{15}$$

where g_j are the coupling strengths between the edge spins and the boundary reservoirs in units of frequency and γ_j and ω_c^j, $j = 1, 2$, are the widths and the peak frequencies of each distribution, respectively.

For analytical simplification of Eq. (7), we extend the lower limit of the integration over frequency from zero to $-\infty$. Note that such an extension is not, in general, valid for any spectral density; it is, however, well justified in the case of a Lorentzian spectral density with positive peak frequency and width such that the distribution has a practically negligible extension to negative frequencies. The necessary condition for this is $\gamma_j \ll \omega_c^j$. In this case the frequency integrals can be calculated analytically, yielding

$$\begin{aligned} R_j(t) &= \frac{g_j^2}{\pi} \frac{\gamma_j}{2} \int_{-\infty}^{+\infty} \frac{e^{-i\left(\omega_\lambda^j - \omega_{eg}\right)t}}{\left(\omega_\lambda^j - \omega_c^j\right)^2 + \left(\frac{\gamma_j}{2}\right)^2} d\omega_\lambda^j \\ &= g_j^2 e^{-i\Delta_c^j t} e^{-\frac{\gamma_j}{2}t}, \quad j = 1, 2, \end{aligned} \tag{16}$$

where $\Delta_c^j \equiv \omega_c^j - \omega_{eg}$, $j = 1, 2$. The Laplace transforms of $R_j(t)$ are then given by the expressions

$$B_j(s) = \frac{g_j^2}{s + \frac{\gamma_j}{2} + i\Delta_c^j}, \quad j = 1, 2. \tag{17}$$

Using these expressions of $B_j(s)$, $j = 1, 2$, we can easily obtain the time evolution of the amplitudes $\tilde{c}_i(t)$, $i, \ldots, N$, using Eqs. (9), (11), and (14). Note that in all of our calculations, we express all couplings entering the formalism in units of the nearest-neighbor coupling strength $\mathcal{J}$. Thus, in our figures, time is measured in the dimensionless units $\mathcal{J}t$.

In Fig. 2(a) we study the dynamics of the populations of the edge as well as the intermediate spins in the $g_1, g_2 < \mathcal{J}$ case for $c_1(0) = 1$. For the intermediate qubits, we adopt the term "channel qubits," which is frequently used in quantum information protocols and represents the sum of the populations of all except the two edge qubits. The corresponding occupation probability is $P_{Ch}(t) = \sum_{i=2}^{N-1} |c_i(t)|^2 = \sum_{i=2}^{N-1} |\tilde{c}_i(t)|^2$. Since the coupling between the qubits is larger than the couplings between the edge spins and the reservoirs, we observe oscillations in the edge and channel qubit populations, associated with the spreading of the initial excitation throughout the whole chain. Eventually, the population will be lost due to the environmental dissipation. This can be seen through the long-time dynamical picture of the sum of all qubit populations, as in Fig. 2(c). On the other hand, in the case where $g_1, g_2 > \mathcal{J}$, as examined in Fig. 2(b), since the initial excitation is on the first qubit, the population is essentially "trapped," albeit not permanently, between the first qubit and environment 1, with only a small portion of the population leaking to the channel.

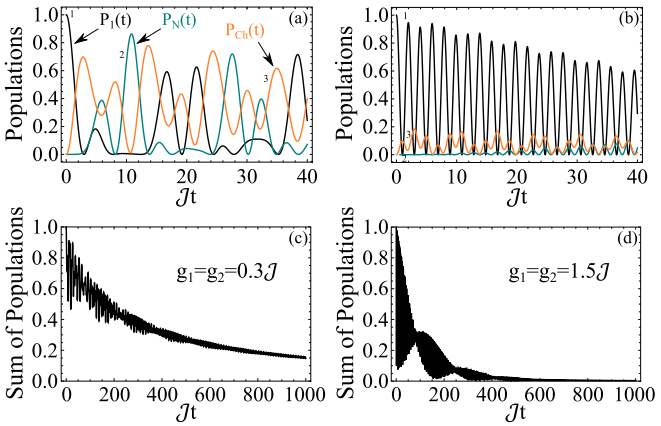

FIG. 2. Dynamics of the populations of the first qubit (black line)[1], Nth qubit (teal line)[2], and channel qubits (orange line)[3] for $c_1(0) = 1$, $N = 5$, $\gamma_1 = \gamma_2 = 0.02\mathcal{J}$, $\Delta_c^1 = \Delta_c^2 = 0$, and (a) $g_1 = g_2 = 0.3\mathcal{J}$ and (b) $g_1 = g_2 = 1.5\mathcal{J}$. In (c) and (d) we show the long-time dynamics of the sum of all qubit populations in the spin chain for $g_1 = g_2 = 0.3\mathcal{J}$ and $g_1 = g_2 = 1.5\mathcal{J}$, respectively.

In this case the exact value of g_2 is of little relevance since the population of the Nth site at any time t is practically negligible. As seen in Fig. 2(d), the strong coupling between the first qubit and the reservoir causes the total population to be lost through the reservoir much faster than in the previous case.

Although, as discussed above, the strong coupling between the environment and the edge qubits may result in population trapping [Fig. 2(b)], if the chain length is small (up to five qubits or so), the long-time dynamics of the chain reveals an oscillatory population transfer between the two edges of the chain (Fig. 3) along with the dissipation to the reservoirs. In that case, the population of the $N - 2$ channel qubits remains low for any time t [see insets in Figs. 3(a)–3(c)]. This effect ceases to occur for spin chains of longer length since the excitation cannot be easily transferred between the two edges of the chain. As seen in Fig. 3, the frequency of these oscillation is highly sensitive to N, decreasing as the latter increases.

In Fig. 4 we examine the long-time dynamics of the total population for chains with an odd number of sites and initial excitation on the center of the chain, i.e., $c_{(N+1)/2}(0) = 1$. In Figs. 2(c) and 2(d) we observe that, if the initial excitation is on the first qubit, the total population of the chain decays much faster for increasing values of g_1. This, of course, is also true for $c_N(0) = 1$ and increasing values of g_2, which is also obvious from symmetry arguments. However, as seen in Fig. 4(a), if the initial excitation is on the center of the chain, increasing the magnitude of the couplings between the edge spins and the corresponding environment leads to the completely opposite effect, namely, a much slower decay of the total population in the long-time dynamics picture. Such an effect occurs only as long as the boundary couplings are larger than the coupling between the qubits $\mathcal{J}$. In the opposite regime, the increase of the boundary couplings (to values still less than $\mathcal{J}$) results in faster decay of the total population to the reservoirs. These results indicate that, for large boundary couplings, the evolution of the edge spins tends

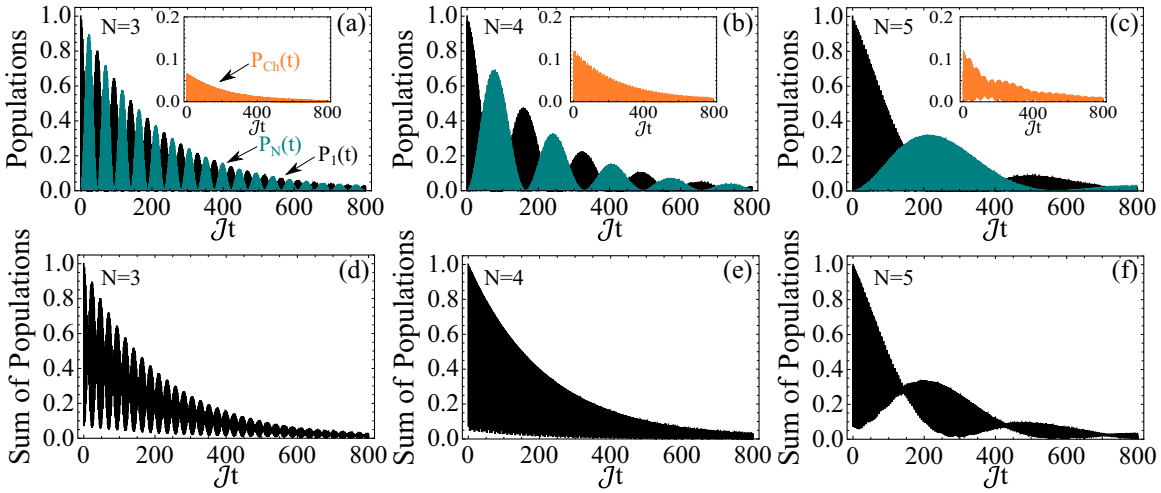

FIG. 3. Long-time dynamics of the populations $P_1(t)$, $P_N(t)$, and $P_{Ch}(t)$ (inset) as well as their sum for spin chains of small length and $c_1(0) = 1$, $\gamma_1 = \gamma_2 = 0.01\mathcal{J}$, $g_1 = g_2 = 1.8\mathcal{J}$, $\Delta_c^1 = \Delta_c^2 = 0$. (a) and (d) $N = 3$, (b) and (e) $N = 4$, and (c) and (f) $N = 5$.

to freeze, alluding to a quantum Zeno effect, leading thus to an effective hindering of the total decay to the reservoirs through them. This hindering of the decay becomes even more pronounced for increasing chain lengths [Fig. 4(b)], which physically can be attributed to the increased number of pathways for the evolution of the initial excitation throughout the whole chain and therefore the smaller likelihood for the population to reach the edge spins and be lost to the reservoirs.

It may be useful at this point to note that the dissipation of the total population to the reservoirs can also be slowed down by choosing detunings Δ_c^1 and Δ_c^2 larger than the boundary-coupling constants. In that regime of parameters, the dominant modes of the Lorentzian spectral densities of the boundary reservoirs are off resonant with the qubit frequency and therefore do damp the system less. That might be argued to be obvious. Be that as it may, the statement is valid only in the context of non-Markovian reservoirs; because the spectral density of a non-Markovian reservoir must, at some frequency, exhibit a more or less pronounced peak, as it must depart from the slowly varying, smooth spectral density which is necessary for the Markovian approximation. It could therefore be viewed as yet another feature of non-Markovian behavior.

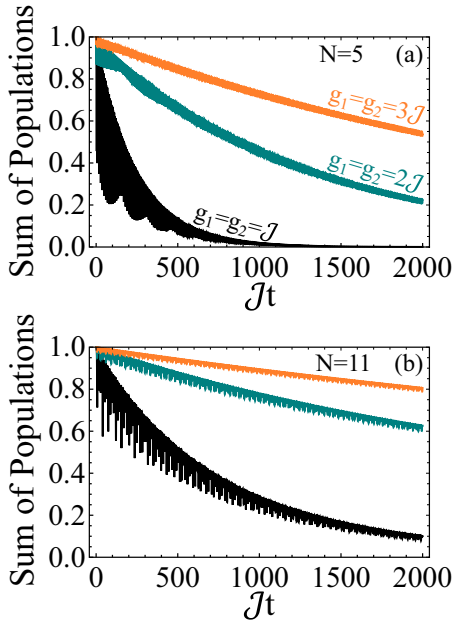

FIG. 4. Long-time dynamics of the sum of all qubit populations in the spin chain with the initial excitation in the central qubit $c_{(N+1)/2}(0) = 1$ and $\gamma_1 = \gamma_2 = 0.02\mathcal{J}$, $\Delta_c^1 = \Delta_c^2 = 0$, and (a) $N = 5$ and (b) $N = 11$. Black line: $g_1 = g_2 = \mathcal{J}$, teal line: $g_1 = g_2 = 2\mathcal{J}$, and orange line: $g_1 = g_2 = 3\mathcal{J}$.

It is also important to note that the effect in which the increased coupling constants between the edge spins and the environments act like a barrier and protect the total population of the chain from decaying to the latter does not necessarily require an initial excitation in the center of the chain. This is just one among the choices of possible initial conditions where this phenomenon occurs. The general rule is that the initial excitation should be anywhere but the edge spins in order to avoid the trapping of the population between the edge spins and their corresponding reservoirs, as was the case in Fig. 2(b). For example, an increase of g_1 and g_2 for a chain system initially prepared in the state $\frac{1}{\sqrt{N-2}}\sum_{i=2}^{N-1}|\psi_i\rangle$ will result in the same phenomenon that occurs in Fig. 4.

In Fig. 5, we study the state-transfer properties between the two edge spins of the chain in terms of the average-state fidelity [54]

$$\mathcal{F}(t) = \frac{1}{2} + \frac{|c_N(t)|^2}{6} + \frac{|c_N(t)|}{3}, \tag{18}$$

which involves an average over all possible sender-qubit states. In Fig. 5(a) we show the dynamics of the average-state fidelity for a spin chain with $N = 10$ sites for different values of the boundary couplings g_1 and g_2. As becomes evident, the first peak of the average-state fidelity is very sensitive to the boundary couplings, decreasing as their values increase. At the same time subsequent peaks in time tend to increase their maximum value. The position of the first peak indicates

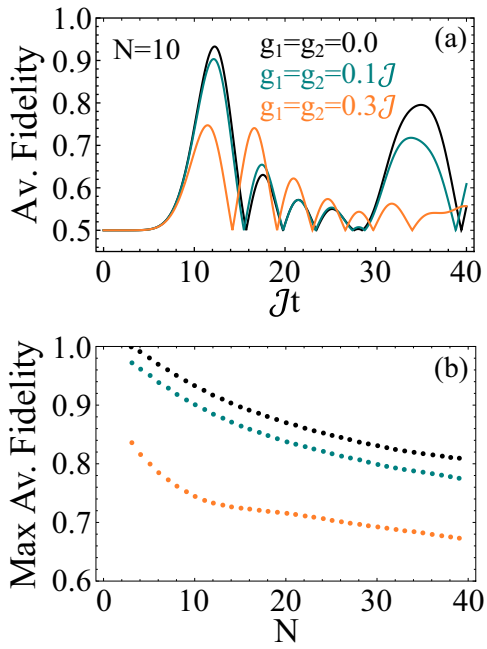

FIG. 5. (a) Dynamics of the average-state fidelity of state transfer between the two edges of the spin chain for $N = 10$ and (b) maximum average fidelity as a function of the number of spin sites N. In both panels $\gamma_1 = \gamma_2 = 0.5\mathcal{J}$, $\Delta_c^1 = \Delta_c^2 = 0$, and $g_1 = g_2 = 0$ (black line or dots), $g_1 = g_2 = 0.1\mathcal{J}$ (teal line or dots), and $g_1 = g_2 = 0.3\mathcal{J}$ (orange line or dots).

that the transfer time is slightly decreased by increasing the boundary couplings; however, larger values of the latter lead to nonfaithful state transfer in general. In Fig. 5(b) we examine the behavior of the maximum value of the average-state fidelity as a function of the number of spin sites for chain length up to 40 sites. As N increases, the maximum average-state fidelity tends towards lower values that depend also on the values of the boundary couplings of the edge spins with the reservoirs. Our results qualitatively agree with a similar study by Ren *et al.* [45], in which they studied the state-transfer properties of the same system using the dephasing and dissipation models in terms of the quantum state diffusion approach.

B. Ohmic spectral density

As a second example, we consider the case of boundary reservoirs characterized by Ohmic spectral densities [55,56], according to the relation

$$J_j(\omega_\lambda^j) = \mathcal{N}_j g_j^2 \omega_c^j \left(\frac{\omega_\lambda^j}{\omega_c^j}\right)^{\mathcal{S}_j} \exp\left(-\frac{\omega_\lambda^j}{\omega_c^j}\right), \quad j = 1, 2, \tag{19}$$

where g_j are qubit-environment coupling constants in units of frequency, ω_c^j are the so-called Ohmic cutoff frequencies, and $\mathcal{S}_j$ $(j = 1, 2)$ are the Ohmic parameters characterizing whether the spectrum of the reservoirs is sub-Ohmic ($\mathcal{S} < 1$), Ohmic ($\mathcal{S} = 1$), or super-Ohmic ($\mathcal{S} > 1$). $\mathcal{N}_j$ is a normalization constant given by the relation $\mathcal{N}_j = \frac{1}{(\omega_c^j)^2\Gamma(1+\mathcal{S}_j)}$, where $\Gamma(z)$ is the gamma function.

Inserting Eq. (19) back into Eq. (7), we perform the integration over frequency for arbitrary $\mathcal{S}_j$ and find that $R_j(t)$ is given by the expression

$$\begin{aligned} R_j(t) &= \mathcal{N}_j g_j^2 \omega_c^j \int_0^\infty \left(\frac{\omega_\lambda^j}{\omega_c^j}\right)^{\mathcal{S}_j} e^{-\frac{\omega_\lambda^j}{\omega_c^j}} e^{-i\left(\omega_\lambda^j - \omega_{eg}\right)t} d\omega_\lambda^j \\ &= g_j^2 e^{i\omega_{eg}t} \left(i\omega_c^j t + 1\right)^{-1-\mathcal{S}_j}, \quad j = 1, 2. \end{aligned} \tag{20}$$

Note that, unlike much of the literature, in our use of Ohmic spectral densities we found it necessary to include the normalization factor $\mathcal{N}_j$, which renders meaningful the comparison with the Lorentzian spectral density, discussed in Sec. III C.

The Laplace transform of Eq. (20) can also be calculated analytically, yielding

$$\begin{aligned} B_j(s) &= -g_j^2 \frac{i^{1-\mathcal{S}_j}}{\omega_c^j} e^{-iK_j(s)} [K_j(s)]^{\mathcal{S}_j} \Gamma(-\mathcal{S}_j, -iK_j(s)), \\ & j = 1, 2, \end{aligned} \tag{21}$$

where $K_j(s) \equiv (s - i\omega_{eg})/\omega_c^j$ $(j = 1, 2)$ and $\Gamma(a, z)$ is the incomplete gamma function. In the special case where $\mathcal{S}_j$ are integers, it is useful to use the incomplete gamma function property

$$\begin{aligned} \Gamma(-n, z) = \frac{1}{n!}\Bigg[&\frac{e^{-z}}{z^n} \sum_{k=0}^{n-1} (-1)^k (n-k-1)! z^k \\ &+ (-1)^n \Gamma(0, z)\Bigg], \end{aligned} \tag{22}$$

which holds for integer n, to express $B_j(s)$ in terms of $\Gamma(0, -iK_j(s))$. Using Eq. (21), as in the previous case, we can easily calculate the Laplace inversion numerically and find the time evolution of the amplitudes $\tilde{c}_i(t)$, $i, \ldots, N$.

In Fig. 6 we study the dynamics of the sum of all qubit populations in the chain for various parameters of the Ohmic reservoirs. The dynamics of this quantity provides us straightforward information on how fast the initial excitation gets lost in the two environments. As Fig. 6(a) indicates, by increasing the Ohmic parameters $\mathcal{S}_j$ $(j = 1, 2)$ of the reservoirs, the sum of populations decays more slowly, indicating a slower decay of the single excitation to the environments. Physically, this effect is attributed to the fact that by increasing $\mathcal{S}_j$, the spectral density distribution of the environments is mainly peaked in the vicinity of modes whose frequency is larger than the qubit frequency $\omega_{eg} = \mathcal{J}$ [see the inset in Fig. 6(b)], and therefore, by being off resonant with the qubit frequency, they damp the system less. A similar behavior is observed in Fig. 6(b), where the dynamics are shown as a function of the cutoff frequencies for the Ohmic type of environments ($\mathcal{S}_j = 1$). Since for Ohmic distributions the peak of the distribution coincides with the cutoff frequency ω_c^j $(j = 1, 2)$, an increase in the cutoff frequencies results in distributions whose modes extend mainly beyond ω_{eg}, resulting in a slower decay to the boundary environments. Note that, in general, for arbitrary Ohmic parameters, the Ohmic distributions are always peaked at the frequencies $\omega_\lambda^j = \mathcal{S}_j \omega_c^j$, $j = 1, 2$. The characteristic oscillations observed in both panels of Fig. 6 are indicative of the non-Markovian character of the Ohmic boundary reservoirs, enabling the exchange of population between them and the spin chain within finite times.

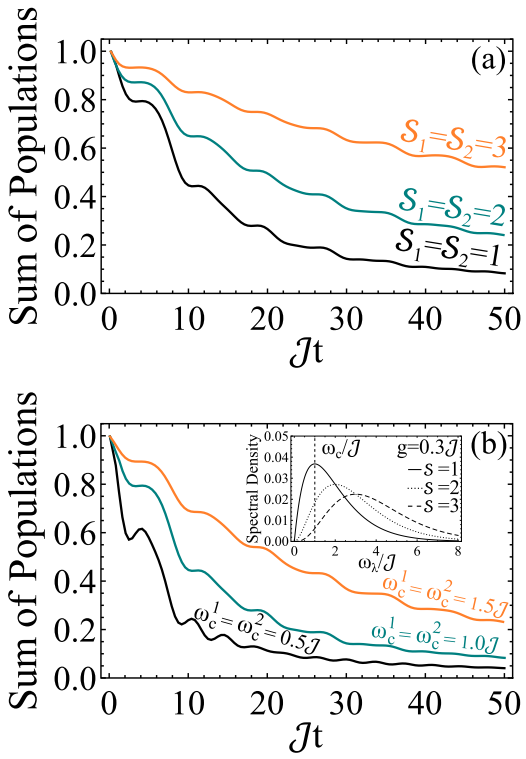

FIG. 6. Dynamics of the sum of all qubit populations in an $N = 6$ qubit chain, boundary-driven by reservoirs with Ohmic spectral densities. The parameters used in (a) are $\omega_c^1 = \omega_c^2 = \mathcal{J}$ and $\mathcal{S}_1 = \mathcal{S}_2 = 1$ (black line), $\mathcal{S}_1 = \mathcal{S}_2 = 2$ (teal line), and $\mathcal{S}_1 = \mathcal{S}_2 = 3$ (orange line), while in (b), $\mathcal{S}_1 = \mathcal{S}_2 = 1$ and $\omega_c^1 = \omega_c^2 = 0.5\mathcal{J}$ (black line), $\omega_c^1 = \omega_c^2 = 1.0\mathcal{J}$ (teal line), and $\omega_c^1 = \omega_c^2 = 1.5\mathcal{J}$ (orange line). In both panels, $g_1 = g_2 = 0.3\mathcal{J}$, $\omega_{eg} = \mathcal{J}$, and $c_1(0) = 1$. The inset in (b) shows the Ohmic spectral density as a function of ω_λ for various Ohmic parameters $\mathcal{S}$ ($\mathcal{S} = 1$: solid line, $\mathcal{S} = 2$: dotted line, and $\mathcal{S} = 3$: dashed line) and $g = 0.3\mathcal{J}$ (coupling strength) and $\omega_c = \mathcal{J}$ (dotted vertical line).

In Fig. 7(a) we examine the dynamics of the populations of the edge as well as the channel qubits of the chain for Ohmic boundary reservoirs ($\mathcal{S}_j = 1$, $j = 1, 2$) in the weak-boundary-coupling regime $g_1, g_2 < \mathcal{J}$. The initial single excitation is on the first qubit [$c_1(0) = 1$]. The dynamics indicate oscillations between the populations of the chain damped by the two Ohmic environments. The situation, however, may change drastically in the strong-boundary-coupling regime $g_1, g_2 > \mathcal{J}$, as shown in Fig. 7(b). In this case the dynamics of the population $P_1(t)$ indicate a long-time stability behavior around a finite value for times much larger than any other timescale of the system. Note that a further increase of the boundary-coupling constants will not result in the increase of this long-time stability value. Still, as seen in Fig. 7(c), this value is highly affected by the Ohmic parameters of the environments (more specifically, by the Ohmic parameter of the first environment, which is the one that communicates with the first qubit). In general, an increase in the Ohmic parameters results in more complex behavior, as indicated by the orange line in Fig. 7(c). In the long-time dynamics picture, the population of the first qubit exhibits an oscillatory behavior with a frequency that depends on the Ohmic parameter of its boundary reservoir. These noncoherent oscillations become faster for super-Ohmic reservoirs and are essentially an effect associated with the non-Markovianity of the boundary reservoirs that drive the chain since they indicate population exchanges between the chain and the latter for very long times. Another parameter that considerably affects this oscillatory behavior is the number of qubit sites. In Fig. 7(d) we plot the dynamics of $P_1(t)$ for a chain of various numbers of qubit sites N, boundary-driven by super-Ohmic environments with $\mathcal{S}_j = 2$, $j = 1, 2$. For a small number of qubit sites, the long-time dynamics in the inset in Fig. 7(d) indicate a long-living coherent oscillatory behavior (black line), while for chains that consist of a larger number of qubits, the population of the first qubit exhibits small noncoherent oscillations around a stabilized value (orange line). Our results are just a first glimpse of the richness of the effects one may expect from the boundary driving of chains with an Ohmic type of reservoirs.

C. Comparing Lorentzian to Ohmic spectral densities

So far we have separately studied the cases of boundary-driven chains using reservoirs with Lorentzian and Ohmic spectral densities. As is evident throughout our formalism, the dynamics of the chain when the boundary reservoirs are characterized by a Lorentzian spectral density does not depend directly on the qubit frequency ω_{eg} but on the detuning Δ_c between the latter and the peak frequency of the Lorentzian. Therefore, the specification of Δ_c along with the rest of the Lorentzian and spin-chain parameters is sufficient for calculating the wave function of the chain. However, this is not the case for Ohmic boundary reservoirs, where, in order to calculate aspects of the chain dynamics, one must specify the qubit frequency ω_{eg} as well as all of the rest of the Ohmic spectral density parameters (i.e., the cutoff frequency and Ohmic parameter). This direct dependence on the qubit frequency is reflected in the particular form of $B_j(s)$ for Ohmic boundary reservoirs according to Eq. (21). In all of our calculations involving Ohmic boundary reservoirs, in the regime of the parameters we have explored, no couplings are significantly larger than the qubit frequency or the cutoff frequencies ω_c^j, $j = 1, 2$.

In Fig. 8, we provide a comparative evaluation of the effect of the two spectral densities. In Fig. 8(a), we have chosen both distributions to be peaked exactly on resonance with the qubit frequency $\omega_{eg} = 3\mathcal{J}$. Although the freedom in the choice of the parameters of each distribution results in many possible line shapes of their spectral densities, the general tendency for typical parameters of the two distributions is that Ohmic distributions are usually wider than Lorentzian distributions. In Fig. 8(b) we use the distributions of Fig. 8(a) as spectral densities of the boundary reservoirs and study the dynamics of the sum of all qubit populations in an $N = 7$ chain for various values of the boundary couplings g_j, $j = 1, 2$, and initial excitation in the center of the chain. The solid lines correspond to Lorentzian boundary reservoirs, while the dashed lines correspond to the Ohmic ones. As also argued in the discussion of Fig. 4, since the initial excitation is not on the edge qubits of the chain and the boundary couplings are larger than the qubit-qubit coupling $\mathcal{J}$, increasing the values of g_j, $j = 1, 2$, results in slower dissipation of the total excitation in

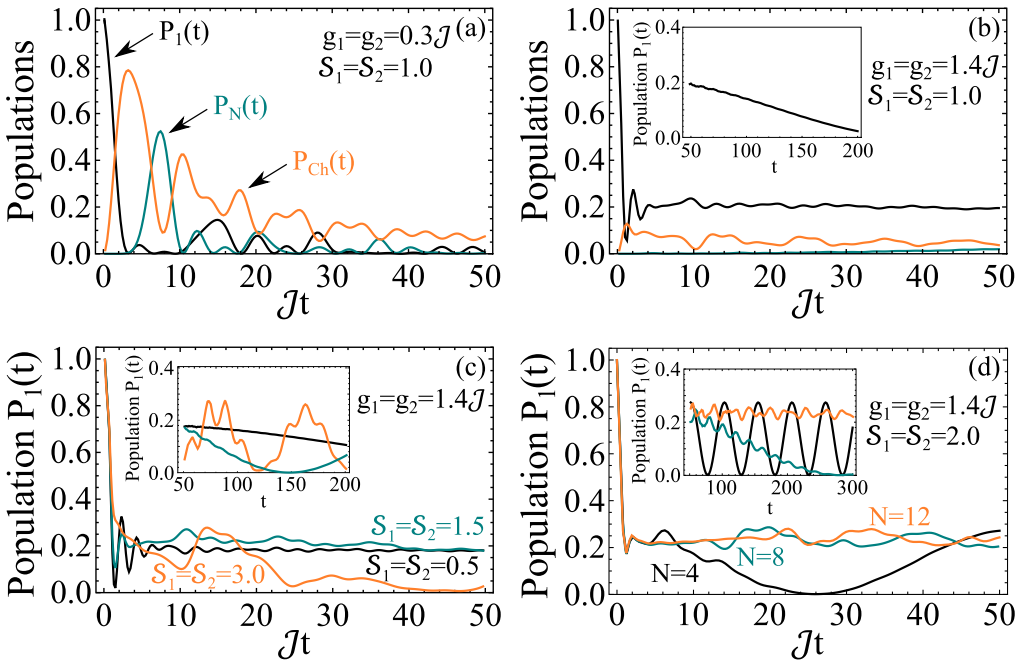

FIG. 7. (a) Dynamics of the populations of the first qubit (black line), Nth qubit (teal line), and channel qubits (orange line) for $c_1(0) = 1$, $N = 6$, $\omega_{eg} = \mathcal{J}$, $\omega_c^1 = \omega_c^2 = \mathcal{J}$, $\mathcal{S}_1 = \mathcal{S}_2 = 1$, and $g_1 = g_2 = 0.3\mathcal{J}$. (b) Same as in (a), but for $g_1 = g_2 = 1.4\mathcal{J}$. (c) Dynamics of the population $P_1(t)$ for various values of the environmental Ohmic parameters and $c_1(0) = 1$, $N = 6$, $\omega_{eg} = \mathcal{J}$, $\omega_c^1 = \omega_c^2 = \mathcal{J}$, $g_1 = g_2 = 1.4\mathcal{J}$. Black line: $\mathcal{S}_1 = \mathcal{S}_2 = 0.5$, teal line: $\mathcal{S}_1 = \mathcal{S}_2 = 1.5$, and orange line: $\mathcal{S}_1 = \mathcal{S}_2 = 3.0$. (d) Dynamics of the population $P_1(t)$ for various values of the number of qubit sites and $c_1(0) = 1$, $\omega_{eg} = \mathcal{J}$, $\omega_c^1 = \omega_c^2 = \mathcal{J}$, $\mathcal{S}_1 = \mathcal{S}_2 = 2.0$, $g_1 = g_2 = 1.4\mathcal{J}$. Black line: $N = 4$, teal line: $N = 8$, and orange line: $N = 12$. In the insets of (b)–(d) we show the long-time dynamics of the population $P_1(t)$.

the environments. A comparison of the solid (Lorentzian) and dashed (Ohmic) lines reveals two major differences: First, the dynamics of the total population in the boundary-driven chain with Lorentzian reservoirs is more sensitive to the increase of the boundary couplings compared to the Ohmic-driven chain. Moreover, for the particular combination of parameters chosen, the total excitation in the chain tends to live longer in Lorentzian-driven chains compared to Ohmic-driven ones, which can be attributed to the much broader profile of the Ohmic spectral density compared to the Lorentzian one. Second, it is evident that the dynamics of the sum of all qubit populations exhibit more vivid oscillations in the Lorentzian case compared to the Ohmic one. Such oscillations are indicative of the non-Markovian character of the boundary reservoirs and therefore the exchange of populations between the chain and the reservoirs within finite times. Even if both types of reservoirs are non-Markovian, the Ohmic spectral density in Fig. 8(a) tends to be substantially flatter than the Lorentzian spectral density, thus resembling a Markovian environment for which no oscillations are expected between the chain and its boundaries.

Finally, before concluding, we should note that the dynamics of the average-state fidelity of the state transfer between the edges of a chain boundary-driven by Ohmic reservoirs displays a behavior more or less qualitatively similar to the corresponding average-state fidelity dynamics of a boundary-driven chain with Lorentzian reservoirs, shown in Fig. 5.

IV. CONCLUDING REMARKS AND OUTLOOK

In this paper, we have presented a formalism for a systematic way of calculating the wave function of an arbitrary-length XX spin chain, boundary-driven by non-Markovian environments of arbitrary spectral density. The theory is cast in terms of Schrödinger's equations of motion within the single-excitation subspace and leads to closed-form solutions for the Laplace transforms of the amplitudes for arbitrary initial conditions using a recursive method. The inversion integrals can easily be calculated numerically (or even analytically in some cases) upon specification of the spectral density of each environment. The calculation of the wave function of the chain within the single-excitation subspace enables the study of a number of interesting properties of the system. As an illustration of the potential of the approach, we have considered Lorentzian and Ohmic spectral densities for the boundary environments and studied aspects of the dynamical and state-transfer properties of the system. Our results demonstrate the memory effects of the non-Markovian environments. The concomitant information exchange between the latter and the spin chain gives rise to a plethora of interesting effects such as population trapping, oscillations between the populations of the edge spins, and the protection of the spin populations against dissipation for increased values of the boundary couplings.

One aspect of our results that turns out to be revealing and somewhat surprising has to do with the comparative analysis of the dynamics of the chain under two quite different reser-

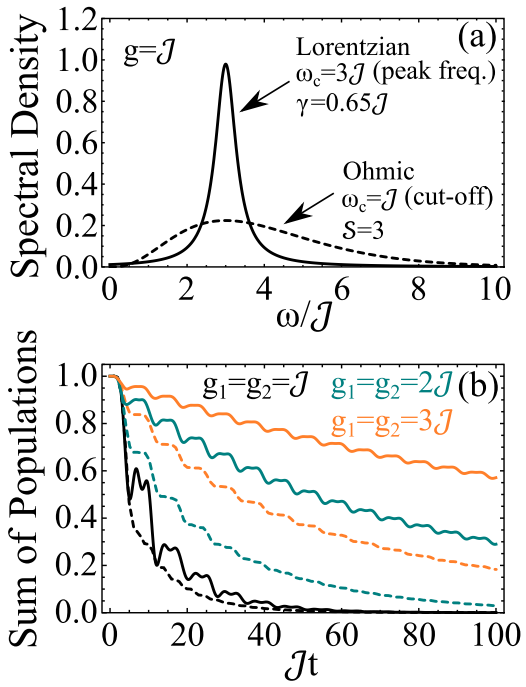

FIG. 8. (a) Spectral density of a Lorentzian distribution with peak frequency $\omega_c = 3\mathcal{J}$, width $\gamma = 0.65\mathcal{J}$, and $g = \mathcal{J}$ (solid line) compared with an Ohmic distribution with Ohmic parameter $\mathcal{S} = 3$, cutoff frequency $\omega_c = \mathcal{J}$, and $g = \mathcal{J}$ (dashed line). (b) Dynamics of the sum of all qubit populations in an $N = 7$ chain and initial excitation in the center of the chain [$c_{(N+1)/2}(0) = 1$] for various coupling strengths between the boundary reservoirs and the edge qubits. Black line: $g_1 = g_2 = \mathcal{J}$, teal line: $g_1 = g_2 = 2\mathcal{J}$, and orange line: $g_1 = g_2 = 3\mathcal{J}$. The solid lines correspond to Lorentzian boundary reservoirs, while the dashed lines correspond to Ohmic ones. The rest of the parameters (except the coupling strengths) correspond to the parameters in (a). The qubit frequency is chosen to be resonant with the peak frequency of the two distributions, namely, $\omega_{eg} = 3\mathcal{J}$.

voirs, namely, Lorentzian and Ohmic. We adopted the general notion that any reservoir with spectral density not smoothly and slowly varying as a function of energy (frequency) within an extended range around the resonance with the qubit is non-Markovian. This entails some degree of memory, which in turn implies that the loss to the reservoir would not be monotonic. In much of the work on and approaches to non-Markovian reservoirs, it is the Lorentzian that has served as a typical illustration. Physically, that behavior should be expected for a Lorentzian spectral density as it exhibits a well-defined peak. But so do Ohmic and super-Ohmic spectral densities. However, our direct quantitative comparison of the effect of a Lorentzian spectral density versus that of a super-Ohmic one in Sec. III C revealed the effects of an almost qualitative difference between the two; the effect of the super-Ohmic one resembles an almost Markovian reservoir, which implies a much lower degree of non-Markovianity. This concrete example complements earlier general formulations of measures of non-Markovian behavior [57].

Our work was motivated by the rapidly growing interest in the field of boundary-driven open quantum systems and, in particular, the need for the development of the necessary analytical or numerical tools for the study of their properties. The results provide the background for a number of extensions, such as accounting for different spin-chain configurations, as well as the theoretical description of the system, within our formal development, beyond the single-excitation. It would, in addition, be interesting to investigate whether the behavior for long times of the edge qubits, which communicate directly with the boundary reservoirs (Fig. 7), could be useful in the survival of long-distance quantum correlations for chains consisting of a large number of qubit sites boundary-driven by Ohmic reservoirs. It should, however, be kept in mind that, from the standpoint of state transfer and quantum information processing, the single-excitation scheme is sufficient. Nevertheless, from the standpoint of statistical-mechanics properties of spin chains connected to non-Markovian environments, extension of the approach beyond the single-excitation subspace is necessary. This represents a compelling and very challenging task, on which we hope to make progress in the near future.

Extension of our work to different spin-chain configurations would provide further insight into the dynamics of systems boundary-driven by non-Markovian environments. On that issue, our approach lends itself to the evaluation of the degree of non-Markovianity of various spectral densities. In the present paper, by comparing the effects of Lorentzian to Ohmic environments as manifested in the time evolution of the system and the concomitant dissipation, we have noted some qualitative features attributable to non-Markovianity. There are, however, quantitative measures of non-Markovianity, such as in [57], among others. Given that there is more than one relevant measure [58], we are in the process of exploring those aspects in the context of our system and expect to report on definitive results in future work.

ACKNOWLEDGMENTS

G.M. would like to acknowledge the Institute of Electronic Structure and Laser (IESL), FORTH, for financially supporting this work through its Research and Development Program ΠΔE00710. We are also grateful to Prof. M. B. Plenio for his critical reading of the manuscript.

APPENDIX

The system of equations (8) is a set of N algebraic equations that can be solved recursively as follows: First, we solve Eq. (8a) for $F_2(s)$ and Eq. (8b) for $F_{i+1}(s)$ to find

$$F_2(s) = (iks)F_1(s) + (ik)B_1(s)F_1(s) - (ik)c_1(0), \tag{A1a}$$

$$F_{i+1}(s) = -F_{i-1}(s) + (iks)F_i(s) - (ik)c_j(0), \quad i = 2, \ldots, N-1, \tag{A1b}$$

where $k \equiv 2/\mathcal{J}$. Using these two relations, we can express each $F_i(s)$ in terms of $F_1(s)$. The first few terms up to $F_6(s)$ can be organized as follows:

$$F_2(s) = (iks)F_1(s) + (ik)B_1(s)F_1(s) - (ik)c_1(0), \tag{A2a}$$

$$F_3(s) = [(iks)^2 - 1]F_1(s) + (iks)(ik)B_1(s)F_1(s) - (ik)[(iks)c_1(0) + c_2(0)], \tag{A2b}$$

$$F_4(s) = [(iks)^3 - 2(iks)]F_1(s) + [(iks)^2 - 1](ik)B_1(s)F_1(s) - (ik)\{[(iks)^2 - 1]c_1(0) + (iks)c_2(0) - c_3(0)\}, \tag{A2c}$$

$$\begin{aligned} F_5(s) = {} & [(iks)^4 - 3(iks)^2 + 1]F_1(s) + [(iks)^3 - 2(iks)](ik)B_1(s)F_1(s) \\ & - (ik)\{[(iks)^3 - 2(iks)]c_1(0) + [(iks)^2 - 1]c_2(0) + (iks)c_3(0) + c_4(0)\}, \end{aligned} \tag{A2d}$$

$$\begin{aligned} F_6(s) = {} & [(iks)^5 - 4(iks)^3 + 3(iks)]F_1(s) + [(iks)^4 - 3(iks)^2 + 1]B_1(s)F_1(s) \\ & - (ik)\{[(iks)^4 - 3(iks)^2 + 1]c_1(0) + [(iks)^3 - 2(iks)]c_2(0) + [(iks)^2 - 1]c_3(0) + (iks)c_4(0) + c_5(0)\}. \end{aligned} \tag{A2e}$$

Careful inspection of the above system of equations reveals that $F_i(s)$ follows a pattern of the form

$$F_i(s) = A_i(s)F_1(s) + A_{i-1}(s)(ik)B_1(s)F_1(s) - (ik)\sum_{n=1}^{i-1} A_{i-n}(s)c_n(0), \quad i = 2, \ldots, N, \tag{A3}$$

where $A_i(s)$ obeys the relation

$$A_{m+2}(s) = (iks)A_{m+1}(s) - A_m(s), \quad m = 1, \ldots, N, \tag{A4}$$

with $A_1(s) = 1$ and $A_2(s) = iks$. The mth term of this sequence is given by

$$A_m(s) = \frac{[(iks) + i\sqrt{k^2s^2 + 4}]^m - [(iks) - i\sqrt{k^2s^2 + 4}]^m}{2^m i\sqrt{k^2s^2 + 4}}, \quad m = 1, \ldots, N. \tag{A5}$$

[1] S. Paganelli, S. Lorenzo, T. J. G. Apollaro, F. Plastina, and G. L. Giorgi, Phys. Rev. A **87**, 062309 (2013).
[2] J. I. Cirac, P. Zoller, H. J. Kimble, and H. Mabuchi, Phys. Rev. Lett. **78**, 3221 (1997).
[3] M. Christandl, N. Datta, A. Ekert, and A. J. Landahl, Phys. Rev. Lett. **92**, 187902 (2004).
[4] C. Di Franco, M. Paternostro, and M. S. Kim, Phys. Rev. Lett. **101**, 230502 (2008).
[5] D. Petrosyan, G. M. Nikolopoulos, and P. Lambropoulos, Phys. Rev. A **81**, 042307 (2010).
[6] N. Y. Yao, L. Jiang, A. V. Gorshkov, Z.-X. Gong, A. Zhai, L.-M. Duan, and M. D. Lukin, Phys. Rev. Lett. **106**, 040505 (2011).
[7] A. K. Pavlis, G. M. Nikolopoulos, and P. Lambropoulos, Quantum Inf. Process. **15**, 2553 (2016).
[8] A. Gratsea, G. M. Nikolopoulos, and P. Lambropoulos, Phys. Rev. A **98**, 012304 (2018).
[9] M. B. Plenio, J. Hartley, and J. Eisert, New. J. Phys. **6**, 36 (2004).
[10] S. Bose, Phys. Rev. Lett. **91**, 207901 (2003).
[11] L. Campos Venuti, S. M. Giampaolo, F. Illuminati, and P. Zanardi, Phys. Rev. A **76**, 052328 (2007).
[12] S. M. Giampaolo and F. Illuminati, New J. Phys. **12**, 025019 (2010).
[13] S. Sahling, G. Remenyi, C. Paulsen, P. Monceau, V. Saligrama, C. Marin, A. Revcolevschi, L. P. Regnault, S. Raymond, and J. E. Lorenzo, Nat. Phys. **11**, 255 (2015).
[14] M. P. Estarellas, I. D'Amico, and T. P. Spiller, Phys. Rev. A **95**, 042335 (2017).
[15] F. Plastina and T. J. G. Apollaro, Phys. Rev. Lett. **99**, 177210 (2007).
[16] T. Yu and J. H. Eberly, Phys. Rev. Lett. **93**, 140404 (2004); **97**, 140403 (2006); J. H. Eberly and T. Yu, Science **316**, 555 (2007).
[17] M. P. Almeida, F. de Melo, M. Hor-Meyll, A. Salles, S. P. Walborn, P. H. Souto Ribeiro, and L. Davidovich, Science **316**, 579 (2007).
[18] J. Laurat, K. S. Choi, H. Deng, C. W. Chou, and H. J. Kimble, Phys. Rev. Lett. **99**, 180504 (2007).
[19] P. Marek, J. Lee, and M. S. Kim, Phys. Rev. A **77**, 032302 (2008).
[20] A. Al-Qasimi and D. F. V. James, Phys. Rev. A **77**, 012117 (2008).
[21] M. B. Plenio and S. F. Huelga, New J. Phys. **10**, 113019 (2008).
[22] Z. Lan, L. Jing, and S. Tao, Commun. Theor. Phys. **52**, 226 (2009).
[23] Z.-M. Wang, F.-H. Ren, D.-W. Luo, Z.-Y. Yan, and L.-A. Wu, J. Phys. A **54**, 155303 (2021).
[24] S. R. Clark, J. Prior, M. J. Hartmann, D. Jaksch, and M. B. Plenio, New J. Phys. **12**, 025005 (2010).
[25] M. R. Pourkarimi, M. Rahnama, and H. Rooholamini, Int. J. Theor. Phys. **54**, 1085 (2015).
[26] Z.-Y. Sun, K.-L. Yao, W. Yao, D.-H. Zhang, and Z.-L. Liu, Phys. Rev. B **77**, 014416 (2008).
[27] G. Sadiek and S. Almalki, Phys. Rev. A **94**, 012341 (2016).
[28] M. Rafiee, Eur. Phys. J. D **72**, 152 (2018).
[29] B. Bellomo, R. Lo Franco, and G. Compagno, Phys. Rev. Lett. **99**, 160502 (2007).
[30] R. Lo Franco, B. Bellomo, S. Maniscalco, and G. Compagno, Int. J. Mod. Phys. B **27**, 1345053 (2013).
[31] T. Ramos, B. Vermersch, P. Hauke, H. Pichler, and P. Zoller, Phys. Rev. A **93**, 062104 (2016).

[32] F. Liu, X. Zhou, and Z.-W. Zhou, Phys. Rev. A **99**, 052119 (2019); **100**, 019901(E) (2019).
[33] Z.-M. Wang, F.-H. Ren, D.-W. Luo, Z.-Y. Yan, and L.-A. Wu, Phys. Rev. A **102**, 042406 (2020).
[34] G. Mouloudakis and P. Lambropoulos, Quantum Inf. Process. **20**, 331 (2021).
[35] H.-P. Breuer, E.-M. Laine, J. Piilo, and B. Vacchini, Rev. Mod. Phys. **88**, 021002 (2016).
[36] G. T. Landi, D. Poletti, and G. Schaller, arXiv:2104.14350.
[37] K. Yamanaka and T. Sasamoto, arXiv:2104.11479.
[38] E. Mascarenhas, G. Giudice, and V. Savona, Quantum **1**, 40 (2017).
[39] A. Dhar, K. Saito, and P. Hanggi, Phys. Rev. E **85**, 011126 (2012).
[40] M. Znidaric, Phys. Rev. Lett. **112**, 040602 (2014).
[41] F. Barra, Sci. Rep. **5**, 14873 (2015).
[42] A. Levy and R. Kosloff, Europhys. Lett. **107**, 20004 (2014).
[43] G. De Chiara, G. Landi, A. Hewgill, B. Reid, A. Ferraro, A. J. Roncaglia, and M. Antezza, New J. Phys. **20**, 113024 (2018).
[44] N. Li, J. Ren, L. Wang, G. Zhang, P. Hanggi, and B. Li, Rev. Mod. Phys. **84**, 1045 (2012).
[45] F.-H. Ren, Z.-M. Wang, and Y.-J. Gu, Quantum Inf. Process. **18**, 193 (2019).
[46] D. Jaschke, M. L. Wall, and L. D. Carr, Comput. Phys. Commun. **225**, 59 (2018).
[47] R. Finsterhölzl, M. Katzer, A. Knorr, and A. Carmele, Entropy **22**, 984 (2020).
[48] M. Znidaric, J. Phys. A **43**, 415004 (2010).
[49] D. Karevski, V. Popkov, and G. M. Schutz, Phys. Rev. Lett. **110**, 047201 (2013).
[50] T. Prosen, Phys. Rev. Lett. **106**, 217206 (2011).
[51] T. Prosen, Phys. Rev. Lett. **107**, 137201 (2011).
[52] M. Michel, J. Gemmer, and G. Mahler, Eur. Phys. J. B **42**, 555 (2004).
[53] H. Wichterich, M. J. Henrich, H.-P. Breuer, J. Gemmer, and M. Michel, Phys. Rev. E **76**, 031115 (2007).
[54] G. M. Nikolopoulos and I. Jex, *Quantum State Transfer and Network Engineering*, Quantum Science and Technology (Springer, Berlin, 2014).
[55] A. J. Leggett, S. Chakravarty, A. T. Dorsey, M. P. A. Fisher, A. Garg, and W. Zwerger, Rev. Mod. Phys. **59**, 1 (1987); **67**, 725 (1995).
[56] U. Weiss, *Quantum Dissipative Systems* (World Scientific, Singapore, 2001).
[57] H.-P. Breuer, E.-M. Laine, and J. Piilo, Phys. Rev. Lett. **103**, 210401 (2009).
[58] J. Dajka, J. Luczka, and P. Hanggi, Phys. Rev. A **84**, 032120 (2011).